

Radial velocity moments of dark matter haloes

Radosław Wojtak¹, Ewa L. Łokas², Stefan Gottlöber³ and Gary A. Mamon^{4,5}

¹*Astronomical Observatory, Jagiellonian University, Orla 171, 30-244 Cracow, Poland, radek_wojtak@o2.pl*

²*Nicolaus Copernicus Astronomical Center, Bartycka 18, 00-716 Warsaw, Poland, lokas@camk.edu.pl*

³*Astrophysikalisches Institut Potsdam, An der Sternwarte 16, 14482 Potsdam, Germany, sgottloeber@aip.de*

⁴*Institut d’Astrophysique de Paris (CNRS UMR 7095), 98 bis Bd Arago, F-75014 Paris, France, gam@iap.fr*

⁵*GEPI (CNRS UMR 8111), Observatoire de Paris, F-92195 Meudon, France*

7 October 2018

ABSTRACT

Using cosmological N -body simulations we study the radial velocity distribution in dark matter haloes focusing on the lowest-order even moments, dispersion and kurtosis. We determine the properties of ten massive haloes in the simulation box approximating their density distribution by the NFW formula characterized by the virial mass and concentration. We also calculate the velocity anisotropy parameter of the haloes and find it mildly radial and increasing with distance from the halo centre. The radial velocity dispersion of the haloes shows a characteristic profile with a maximum, while the radial kurtosis profile decreases with distance starting from a value close to Gaussian near the centre. We therefore confirm that dark matter haloes possess intrinsically non-Gaussian, flat-topped velocity distributions. We find that the radial velocity moments of the simulated haloes are quite well reproduced by the solutions of the Jeans equations obtained for the halo parameters with the anisotropy measured in the simulations. We also study the radial velocity moments for a composite cluster made of ten haloes out to ten virial radii. In this region the velocity dispersion decreases systematically to reach the value of the background, while kurtosis increases from below to above the Gaussian value of 3 signifying a transition from a flat-topped to a strongly peaked velocity distribution with respect to the Gaussian, which can be interpreted as the dominance of ordered flow with a small dispersion. We illustrate the transition by showing explicitly the velocity distribution of the composite cluster in a few radial bins.

Key words: methods: N -body simulations – methods: analytical – galaxies: clusters: general – galaxies: kinematics and dynamics – cosmology: dark matter

1 INTRODUCTION

The density distribution of bound structures has been a subject of vigorous research in recent years. An NFW (Navarro, Frenk & White 1997) density profile was established as a universal formula describing dark matter haloes in large mass range arising in cosmological N -body simulations (for recent refinements see Navarro et al. 2004; Diemand, Moore & Stadel 2004a; Tasitsiomi et al. 2004; Merritt et al. 2005). Much less attention has been devoted to the velocity distribution in bound structures, although it also carries substantial amount of information about the formation and evolution of structure in the Universe. The moments of the velocity distribution in particular proved extremely useful in studies of mass distribution in galaxies and clusters (Kronawitter et al. 2000; van der Marel et al. 2000; Łokas & Mamon 2003).

Recently a few groups studied the velocity distribution of simulated haloes showing, for example, that it departs significantly from a Gaussian distribution expected for virialized objects (Kazantzidis et al. 2004; Sanchis, Łokas & Mamon 2004; Diemand Moore & Stadel 2004b). Such behaviour, manifesting itself in a form of kurtosis value lower than 3, was also seen in real objects like the Coma cluster (Łokas & Mamon 2003) or the Draco dwarf (Łokas, Mamon & Prada 2004). There have been few attempts to provide a theoretical explanation for departures from Gaussianity; it turns out however that weakly non-Gaussian velocity distributions arise naturally in Jeans theory of equilibrium structures (Merrifield & Kent 1990; Łokas 2002; Kazantzidis et al. 2004). Hansen et al. (2004) have shown that the flattened velocity distribution can also be interpreted in terms of Tsallis statistics.

In this Letter we study the radial velocity distribution of dark matter haloes resulting from cosmological N -body simulations focusing on the most useful even moments, the dispersion and kurtosis. We show that they are quite well reproduced by the solutions of the Jeans equations. We also look at the behaviour of the moments outside the virial radius and the overall velocity distribution.

2 THE SIMULATED DARK MATTER HALOES

For this study we run a cosmological dark matter simulation within a box of size $150 h^{-1}$ Mpc assuming the concordance cosmological model (Λ CDM) with parameters $\Omega_M = 0.3$, $\Omega_\Lambda = 0.7$, $h = 0.7$ and $\sigma_8 = 0.9$. We have used a new MPI (Message-Passing Interface) version of the original ART (Adaptive Refinement Tree) code (Kravtsov et al. 1997). The ART code achieves high spatial resolution by refining the underlying uniform grid in all high-density regions with an automated refinement/derefinement algorithm. In the new MPI version of the code the whole simulation box is subdivided into cuboids which contain approximately the same numerical tasks to achieve load balance (not necessarily the same number of particles). Each cuboid is handled by one node of the computer using internal OpenMP parallelization. At the given node the remaining box is evolved using more massive particles as described for the multi-mass version of the ART code (Klypin et al. 2001). This procedure minimizes the communication between nodes. After each basic integration step the borders of the cuboids can be moved if load balance changes. The simulation used 256^3 particles, therefore it achieved a mass resolution of $1.7 \times 10^{10} h^{-1} M_\odot$. The basic grid of the simulation was 256, the maximum refinement level was 6. Therefore, the force resolution (2 cells) reached $18 h^{-1}$ kpc.

The halos have been identified using the hierarchical friends-of-friends (HFOF) algorithm (Klypin et al. 1999) using different linking lengths. The linking length of $b = 0.17$ extracts haloes with masses close to the virial mass for our cosmological model. (We define the virial mass and radius as those with mean density $\Delta_c = 101.9$ times the critical density, see Lokas & Hoffman 2001.) However, the FOF method is known to connect particles along thin bridges which are likely to be broken once the linking parameter is changed. This also means that the shape of structure formed by linked particles differs strongly from spherical and the centre of a halo does not necessarily coincide with the region of maximum density.

In order to find points of maximum density we cut out the particles out to a virial radius (assuming that the FOF mass is equal to the virial mass) and calculate the centres of mass in spheres of decreasing radius, each time making the centre of mass the new halo centre. The centres determined in this way agree very well with centres found with much smaller linking lengths which pick up regions of higher density. We then determine the new masses and virial radii of the haloes by summing up masses of all particles found inside the virial radius defined as before but now measured with respect to the new centre. Choosing the haloes for the analysis we have generally taken the most massive objects found in the simulation box. We have, however, rejected those undergoing a major merger with two or more sub-haloes of comparable mass which would significantly depart

Table 1. Properties of the simulated haloes.

Halo	M_v [$10^{14} M_\odot$]	r_v [Mpc]	c
1	7.49	2.33	5.968
2	7.04	2.29	10.098
3	6.83	2.26	5.360
4	6.49	2.23	8.301
5	5.87	2.15	6.285
6	5.35	2.08	10.320
7	4.82	2.02	8.577
8	4.25	1.93	3.552
9	3.86	1.87	7.607
10	3.54	1.82	7.424

from equilibrium. Within the virial radius, the haloes typically have a few times 10^4 particles. The virial masses and radii of the haloes, M_v and r_v , are listed in Table 1.

For each of the ten haloes we determined its density profile taking averages in radial bins of equal logarithmic length up to the virial radius. The data points obtained in this way were assigned errors estimated as Poisson fluctuations. The measured density profiles are well approximated by the NFW formula (Navarro et al. 1997) $\rho(s)/\rho_{c,0} = \Delta_c c^2 g(c)/[3s(1+cs)^2]$ where $s = r/r_v$, $\rho_{c,0}$ is the present critical density, $\Delta_c = 101.9$ is the characteristic density parameter, c is the concentration parameter and $g(c) = [\ln(1+c) - c/(1+c)]^{-1}$. Fitting this formula to our measured density profiles we determined the concentration parameters of the haloes which are listed in Table 1. Our estimated concentrations are consistent with the dependence of c on mass inferred from N -body simulations by Bullock et al. (2001), also run with a Λ CDM cosmology.

In the following, all velocities will be calculated with respect to the mean velocity inside the virial radius of a given halo. For each halo we measure the mean radial velocity (with the Hubble flow added) of dark matter particles enclosed in shells of thickness $0.1r_v$ centered at $0.05r_v$, $0.15r_v$ etc. assuming a convention that the negative sign indicates infall motion towards the centre of the halo and normalizing to $V_v = (GM_v/r_v)^{1/2}$, the circular velocity at r_v . For a fully virialized object the mean radial velocity should be zero. We find that the measured values are consistent on average with zero inside r_v for most haloes, although some radial variations caused by internal streaming motions are present. They do not exceed $0.4V_v$ however, indicating a rather relaxed state of the objects.

We then average our measurements calculating the mean and dispersion of the measurements for the ten haloes in the corresponding bins. The results are plotted in the upper left panel of Fig. 1 with thicker solid line showing the mean and the two thinner lines indicating the dispersion with respect to the mean. The upper right panel of Fig. 1 shows the radial profile of the anisotropy parameter

$$\beta = 1 - \frac{\sigma_t^2(r)}{2\sigma_r^2(r)} \quad (1)$$

averaged in the same way over the ten haloes, where $\sigma_t^2 = \sigma_\theta^2 + \sigma_\phi^2$ and $\sigma_{\theta,\phi}$ and σ_r are the angular and radial velocity dispersions with respect to the mean velocities. As we can see, the orbits are mildly radial, with positive mean β .

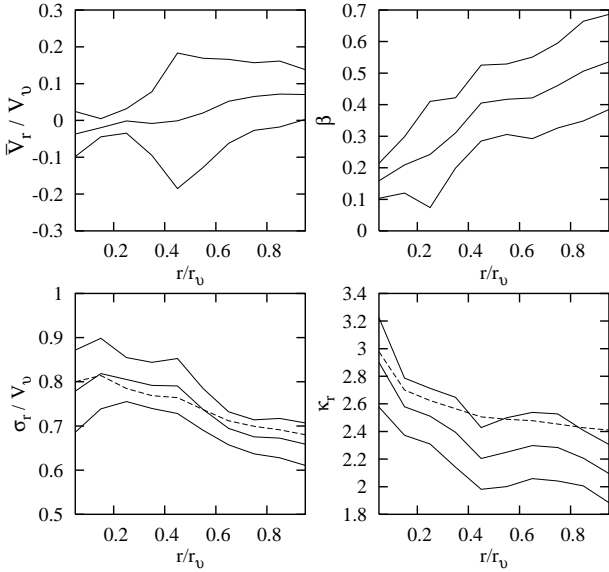


Figure 1. The mean radial velocity in units of V_v , the circular velocity at r_v (upper left panel), the radial profile of the anisotropy parameter β (upper right panel) and the radial moments: velocity dispersion σ_r in units of V_v (lower left panel) and kurtosis κ_r (lower right panel) inside r_v averaged over ten haloes listed in Table 1. Thicker solid lines show the mean and the thinner solid lines the dispersion in the measurements. Dashed lines give predictions from the Jeans equations for $c = 7.4$ and a variable β changing as shown in the upper right panel.

The dispersions needed for the calculation of β were approximated by $\sigma = S$ where S^2 is the most natural estimator of the variance from a large sample of n velocities v_i

$$S^2 = \frac{1}{n} \sum_{i=1}^n (v_i - \bar{v})^2 \quad (2)$$

where $\bar{v} = (\sum_{i=1}^n v_i)/n$ is the mean of velocities in the shell. The lower left panel of Fig. 1 shows the radial velocity dispersion calculated in the same way. In the lower right panel of Fig. 1 we plot the fourth radial velocity moment normalized by the variance squared, i.e. the kurtosis

$$K = \frac{\frac{1}{n} \sum_{i=1}^n (v_i - \bar{v})^4}{(S^2)^2}. \quad (3)$$

Although the moments show a significant scatter from halo to halo and some variability due to substructure in every halo, the overall trend in their behaviour, shown by the mean values plotted in Fig. 1, is clearly visible. In particular, the slightly increasing and then decreasing velocity dispersion profile agrees well with the predictions of Lokas & Mamon (2001) for the NFW haloes. The trend observed in the behaviour of kurtosis which decreases from a value close to 3 (characteristic of a Gaussian distribution) to values well below 3 suggests a flat-topped velocity distribution in the outer radial bins.

3 COMPARISON WITH PREDICTIONS FROM THE JEANS FORMALISM

The Jeans formalism (e.g. Binney & Tremaine 1987) relates the velocity moments of a gravitationally bound object to the underlying mass distribution. We summarize here the

formalism, as developed in Lokas (2002) and Lokas & Mamon (2003). The second σ_r^2 and fourth-order $\overline{v_r^4}$ radial velocity moments obey the Jeans equations

$$\frac{d}{dr}(\nu\sigma_r^2) + \frac{2\beta}{r}\nu\sigma_r^2 + \nu\frac{d\Phi}{dr} = 0 \quad (4)$$

$$\frac{d}{dr}(\nu\overline{v_r^4}) + \frac{2\beta}{r}\nu\overline{v_r^4} + 3\nu\sigma_r^2\frac{d\Phi}{dr} = 0 \quad (5)$$

where ν is the 3D density distribution of the tracer population (here it is the same as the total mass density) and Φ is the gravitational potential, which for an NFW density distribution is $\Phi(s)/V_v^2 = -g(c)\ln(1+cs)/s$. The second equation was derived assuming the distribution function of the form $f(E, L) = f_0(E)L^{-2\beta}$ and the anisotropy parameter β , equation (1), to be constant with radius. We will consider here $-\infty < \beta \leq 1$ which covers all interesting possibilities from radial orbits ($\beta = 1$) to isotropy ($\beta = 0$) and circular orbits ($\beta \rightarrow -\infty$).

The solutions to equations (4)-(5) for $\beta = \text{const}$ are

$$\nu(r)\sigma_r^2(r) = r^{-2\beta} \int_r^\infty x^{2\beta}\nu(x)\frac{d\Phi}{dx} dx \quad (6)$$

$$\nu(r)\overline{v_r^4}(r) = 3r^{-2\beta} \int_r^\infty x^{2\beta}\nu(x)\sigma_r^2(x)\frac{d\Phi}{dx} dx. \quad (7)$$

After introducing expression (6) into (7) and inverting the order of integration in (7) the expression for the fourth moment reduces to a single integral

$$\nu(r)\overline{v_r^4}(r) = 3r^{-2\beta} \int_r^\infty x^{2\beta}\nu(x)\frac{d\Phi}{dx}[\Phi(x) - \Phi(r)] dx. \quad (8)$$

For the specific case of NFW-distributed dark matter particles tracing their own gravitational potential the formulae reduce to the following expressions which can be easily calculated numerically

$$\frac{\sigma_r^2(s)}{V_v^2} = s^{1-2\beta}(1+cs)^2g(c) \quad (9)$$

$$\times \int_s^\infty \frac{z^{2\beta-3}}{(1+cz)^2} \left[\ln(1+cz) - \frac{cz}{1+cz} \right] dz$$

$$\frac{\overline{v_r^4}(s)}{V_v^4} = 3s^{1-2\beta}(1+cs)^2g^2(c) \quad (10)$$

$$\times \int_s^\infty \frac{z^{2\beta-3}}{(1+cz)^2} \left[\ln(1+cz) - \frac{cz}{1+cz} \right]$$

$$\times \left[\frac{\ln(1+cs)}{s} - \frac{\ln(1+cz)}{z} \right] dz$$

where the distances were expressed in units of the virial radius ($s = r/r_v$, $z = x/r_v$) and V_v is the circular velocity at the virial radius. As usual, we express the fourth-order moment in terms of the dimensionless radial kurtosis

$$\kappa_r(r) = \frac{\overline{v_r^4}(r)}{\sigma_r^4(r)}. \quad (11)$$

Although the velocity dispersion profile depends on the concentration parameter (see Lokas & Mamon 2001), our simulated haloes all have similar concentration, so for the comparison with the predictions from the Jeans formalism we will adopt their mean concentration of $c = 7.4$ and focus on the dependence on the anisotropy parameter β . Since the anisotropy changes roughly between $\beta = 0$ in the centre and $\beta = 0.6$ at the virial radius, as shown in the upper right

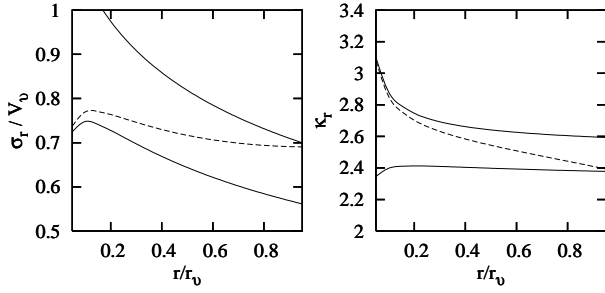


Figure 2. Predicted radial velocity moments for $c = 7.4$ and different β . The left (right) panel shows the radial velocity dispersion σ_r (kurtosis κ_r) for $\beta = 0$ with the lower (upper) solid line and for $\beta = 0.6$ with the upper (lower) solid line. The dashed line in each panel shows the result for β linearly increasing from 0 to 0.6.

panel of Fig. 1, we first plot in Fig. 2 the velocity moments obtained from the solutions (9)-(10) for these two constant values of β . We do not have to restrict our analysis to a constant β however, since the main contribution to $\sigma_r(r)$ and $\kappa_r(r)$ comes from the region close to r in the integrands given in (6)-(7) and the moments are actually sensitive only to a local value of β at a given r . We can therefore reproduce the moments for variable beta taking a different (constant) β for each r . Assuming that β grows linearly between 0 and 0.6 we get results shown with a dashed line in each of the panels in Fig. 2. We see that the new solution changes smoothly from the result for $\beta = 0$ near the centre to the result for $\beta = 0.6$ near the virial radius.

In the lower panels of Fig. 1 we show with dashed lines the predictions from (9)-(10) for β changing as shown in the upper right panel. Namely, as described above, for the calculation of the predicted moments in each bin we assume a value of β found in the same bin after averaging over ten haloes. We can see that the solutions of the Jeans equations reproduce quite well the trends in the behaviour of the radial velocity moments, especially in the case of dispersion. Although the solutions are not formally exact, they do provide fairly good approximations.

4 RADIAL MOMENTS BEYOND THE VIRIAL RADIUS

In this section we extend the analysis beyond the virial radius and look at the behaviour of the moments there. Fig. 3 again shows the same quantities as in Fig. 1 but for a composite cluster made of particles from the ten haloes with distances scaled to r_v of each halo. We plot the measurements up to distances of $10 r_v$, averaged in radial bins of size $0.2 r_v$. The mean radial velocity displays a characteristic behaviour: just outside the virial radius it drops to negative velocities signifying infall, reaches the turn-around radius of the cluster at about $3-4 r_v$ and approaches the Hubble flow at large distances. The velocity dispersion falls to the value characteristic of the background just outside $2 r_v$. The kurtosis falls down inside r_v to values below 3 and then increases sharply at larger distances and oscillates around 5 but staying well above 3. This signifies a velocity distribution which is more peaked in the centre than the Gaussian. The solid line in the upper right panel of the Figure shows the anisotropy parameter defined as in eq. (1). For comparison we also plot with a dashed line the parameter with the con-

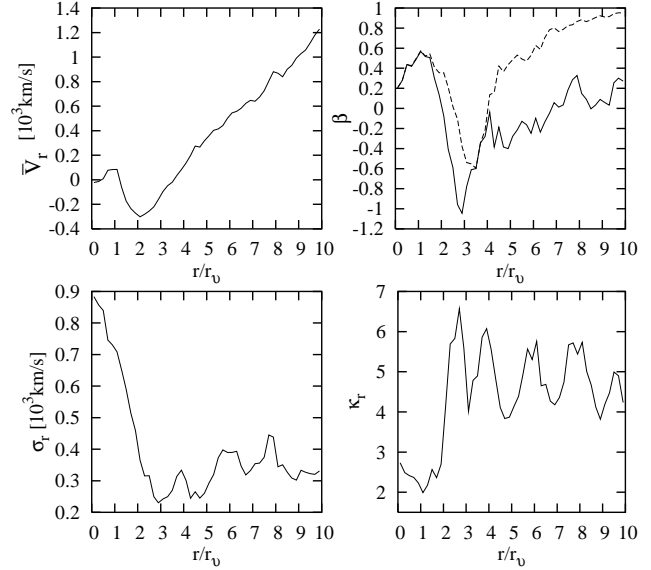


Figure 3. The same quantities as in Fig. 1 measured for a composite cluster made of ten haloes for distances out to $10 r_v$. The dashed line in the upper right panel shows the β parameter including the non-zero mean velocities (see text).

tribution from non-zero mean velocities (i.e. $\beta' = 1 - \overline{v_i^2} / 2\overline{v_i^2}$ where $\overline{v_i^2} = \sigma_i^2 + \overline{v_i^2}$). The anisotropies drop to values below zero outside r_v and approach zero or unity at large distances. This behaviour can be understood as due to dominance of ordered flow in the radial direction outside the virial radius: random motions in the radial direction are smaller while the tangential ones remain the same which results in negative β .

5 SUMMARY AND CONCLUSIONS

We summarize our results by plotting explicitly the radial velocity distribution of our composite cluster in Fig. 4. The histograms shown in the Figure were made for radial bins of equal number (4×10^4) of particles and show their velocity distribution with respect to the mean velocity in each bin. The range of particle positions in each bin (increasing from top to bottom panel) is marked in the corresponding panel. On top of the histograms we plot with dashed lines the normalized Gaussian distributions with dispersions as shown in the lower left panel of Fig. 3.

The first two panels show the distribution inside the virial radius. We can see that the distribution is Gaussian to a very good approximation only in the very centre. In the next bin the distribution is flat-topped with respect to a Gaussian (with the effect becoming systematically stronger when approaching the virial radius). This behaviour is reflected in the decreasing kurtosis profile in the lower right panel of Fig. 1. The distribution shown in the second panel turns out to be quite well fitted by Tsallis distribution $f(v) \propto [1 - (1 - q)(v/v_0)^2]^{q/(1-q)}$ with entropic index $q = 0.65$ and $v_0 = 1178 \text{ km s}^{-1}$ which we show with a solid line (see Lavagno et al. 1998; Hansen et al. 2004).

The third panel shows the velocity distribution in the infall region: the mean velocity of the particles is now negative, but the shape of the distribution is also altered. The distribution is more peaked than a Gaussian signifying a dominance of ordered flow over random motion of particles. The last panel illustrates the velocity distribution in the

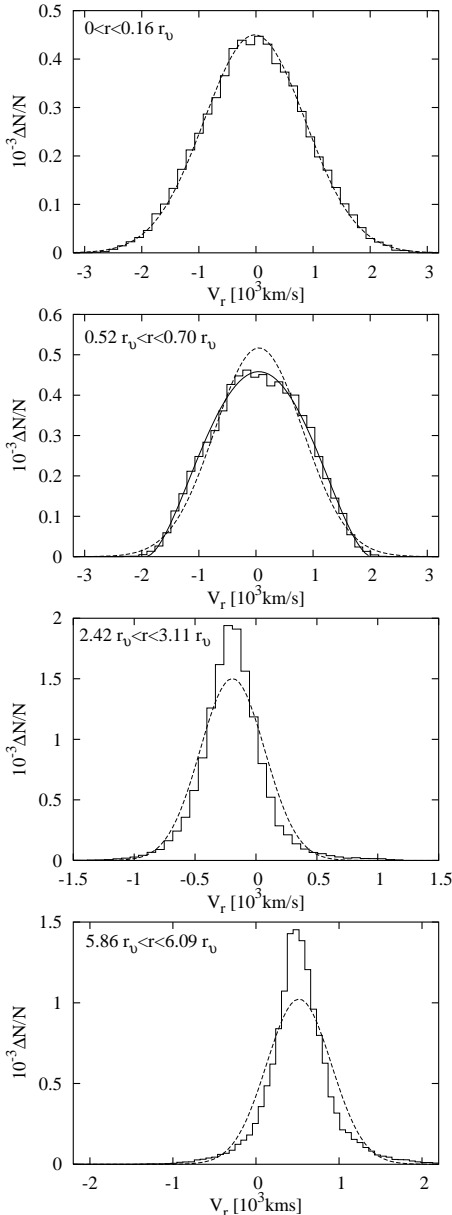


Figure 4. The radial velocity distribution of the composite cluster at different distances. The histograms were made for radial bins of equal number of particles. The range of particle positions in each bin is written in the corresponding panel. On top of the histograms we plot with dashed lines the normalized Gaussian distributions with dispersions measured in a given bin. The solid line in the second panel shows a best-fitting Tsallis distribution with $q = 0.65$.

outflow region, i.e. at distances larger than the turn-around radius. Here the distribution is also more peaked than the Gaussian but the mean velocity of particles is positive.

We have therefore shown that, contrary to the still commonly held belief, the velocity distribution in dark matter haloes is not Gaussian. Except for the very centre, it remains flat-topped inside the virial radius. The transition from the virialized to the non-virialized region is marked by a change in the velocity distribution from flat-topped to strongly peaked with respect to the Gaussian. We have demonstrated that the velocity moments in the virialized re-

gion are quite well reproduced by the solutions of the Jeans equations.

The Gaussian shape of the velocity distribution in the centre is expected since this kind of distribution is characteristic of structures with isothermal density profiles (r^{-2}) and isotropic orbits (Binney & Tremaine 1987; Hansen et al. 2004). Hansen et al. also show that for isotropic orbits steepening of the density profile results in flattening of the velocity distribution, as we observe in our haloes despite the fact that their orbits are mildly radial. It would be very interesting to fully understand the relation between the shape of the distribution and the density profile and anisotropy of particle orbits.

ACKNOWLEDGEMENTS

We wish to thank M. Chodorowski and an anonymous referee for their comments. Computer simulations presented in this paper were performed at the Leibnizrechenzentrum (LRZ) in Munich. RW acknowledges the summer student program at Copernicus Center. RW and EL are grateful for the hospitality of Astrophysikalisches Institut Potsdam where part of this work was done. This research was partially supported by the Polish Ministry of Scientific Research and Information Technology under grant 1P03D02726 as well as the Jumelage program Astronomie France Pologne of CNRS/PAN.

REFERENCES

- Binney J., Tremaine S., 1987, *Galactic Dynamics*. Princeton Univ. Press, Princeton, chap. 4.
- Bullock J. S., Kolatt T. S., Sigad Y., Somerville R. S., Kravtsov A. V., Klypin A. A., Primack J. R., Dekel A., 2001, *MNRAS*, 321, 559
- Diemand J., Moore B., Stadel J., 2004a, *MNRAS*, 353, 624
- Diemand J., Moore B., Stadel J., 2004b, *MNRAS*, 352, 535
- Hansen S. H., Egli D., Hollenstein L., Salzmann C., 2004, *astro-ph/0407111*
- Kazantzidis S., Magorrian J., Moore B., 2004, *ApJ*, 601, 37
- Kravtsov A. V., Klypin A. A., Khokhlov A. M., 1997, *ApJS*, 111, 73
- Kronawitter A., Saglia R. P., Gerhard O., Bender R., 2000, *A&AS*, 144, 53
- Klypin A. A., Gottlöber S., Kravtsov A. V., Khokhlov A. M., 1999, *ApJ*, 516, 530
- Klypin A. A., Kravtsov A. V., Bullock J. S., Primack J. R., 2001, *ApJ*, 554, 903
- Lavagno A., Kaniadakis G., Rego-Monteiro M., Quarati P., Tsallis C., 1998, *ApL&C*, 35, 449, *astro-ph/9607147*
- Lokas E. L., 2002, *MNRAS*, 333, 697
- Lokas E. L., Hoffman Y., 2001, in Spooner N. J. C., Kudryavtsev V., eds, *Proc. 3rd International Workshop, The Identification of Dark Matter*. World Scientific, Singapore, p. 121
- Lokas E. L., Mamon G. A., 2001, *MNRAS*, 321, 155
- Lokas E. L., Mamon G. A., 2003, *MNRAS*, 343, 401
- Lokas E. L., Mamon G. A., Prada F., 2004, *astro-ph/0411694*
- Merrifield M. R., Kent S. M., 1990, *AJ*, 99, 1548
- Merritt D., Navarro J. F., Ludlow A., Jenkins A., 2005, *astro-ph/0502515*
- Navarro J. F., Frenk C. S., White S. D. M., 1997, *ApJ*, 490, 493
- Navarro J. F. et al., 2004, *MNRAS*, 349, 1039
- Sanchis T., Lokas E. L., Mamon G. A., 2004, *MNRAS*, 347, 1198
- Tasitsiomi A., Kravtsov A. V., Gottlöber S., Klypin A. A., 2004, *ApJ*, 607, 125
- van der Marel R. P., Magorrian J., Carlberg R. G., Yee H. K. C., Ellingson E., 2000, *AJ*, 119, 2038